J Mater Sci: Mater Med (2010) 21:99–108
DOI 10.1007/s10856-009-3852-8

Si complexes in calcium phosphate biomaterials

P. Gillespie · Gang Wu · M. Sayer · M. J. Stott

Received: 18 August 2008 / Accepted: 13 August 2009 / Published online: 28 August 2009

Abstract Silicon complexes in silicon doped calcium phosphate bioceramics have been studied using ^{29}Si magic angle spinning nuclear magnetic resonance spectroscopy with the objective of identifying the charge compensation mechanisms of silicon dopants. Three different materials have been studied: a multiphase material composed predominantly of a silicon stabilized α-tricalcium phosphate (α-TCP) phase plus a hydroxyapatite (HA) phase, a single phase Si-HA material and a single phase silicon stabilized α-TCP material. NMR results showed that in all three materials the silicon dopants formed Q^1 structures in which two silicate tetrahedra share an oxygen, creating an oxygen vacancy which compensated the substitution of two silicon for phosphorus. This finding may explain the phase evolution previously found where silicon stabilized α-TCP is found at low temperature after sintering.

1 Introduction

Silicon doped calcium phosphate materials have drawn interest recently as potential bone substitute materials. Silicon doped hydroxyapatite (Si-HA) is the most widely studied of the calcium phosphates due to the similarity between hydroxyapatite (HA,$Ca_5(PO_4)_3OH$) and the inorganic component of bone. Si doping leads to changes in the structural properties of the materials and to a marked improvement in their biological performance but the mechanisms whereby this happens are not fully understood.

Synthetically produced hydroxyapatite and other calcium phosphates have long been considered as potential bioceramics due to their similarity to the inorganic component of bone [1]. These materials react with the physiological environment and form a bond with the surrounding bone tissue [2] which tends to stabilize the implant and enhance healing. However, the reactions that occur between calcium phosphates and biological tissue are fairly slow and occur over a few days, compared to a few minutes with silica based bioglass [3, 4], another promising bone replacement material.

The bioactivity of HA can be enhanced by the addition of a small amount of silicon (around 1 wt%) [2]. These Si-HA materials have been shown to have a greater rate of in vivo dissolution compared to pure HA [5] as well as a greater rate of bone apposition to the surface [6]. A series of studies by Carlisle showed the importance of silicon for skeletal development in baby chicks [7] and an increased concentration of silicon in young, actively growing bones [8] which led to the conclusion that silicon should be classified as an essential trace element for bone development. The high bioactivity observed in silica based glasses has been proposed to be mediated by the formation of silanol groups (Si–OH) on the surface [2].

Another promising bone substitute material is a mixed phase silicon substituted calcium phosphate which has been formed both as a thin film on a quartz substrate [9, 10] as well as a bulk powder [11]. These materials have a phase composition of approximately 75 wt% silicon stabilized α-tricalcium phosphate (TCP) with the rest being predominantly an HA phase with a small quantity of β-TCP, and exhibit a microporous surface morphology due to a network of interconnected particles. It is likely that the HA

P. Gillespie · M. Sayer · M. J. Stott (✉)
Department of Physics, Queen's University, Kingston, Canada
e-mail: stott@mjs.phy.queensu.ca

G. Wu
Department of Chemistry, Queen's University, Kingston, Canada

phase is also doped with Si, although this has not been confirmed experimentally. The materials exhibit a unique biological response by fully participating in the bone remodeling process. In addition to bone apposition these materials are resorbed over time by bone cells and replaced by natural bone [9, 10, 12, 13]. Surprisingly, the majority α-TCP phase is the high temperature TCP phase, with the β phase being typically found at room temperature. The addition of silicon stabilizes α-TCP at lower temperatures and this phase plays a prominent role in the unique biological properties of the material. The bulk form of this material was produced by Millenium Biologix Inc. under the trade name Skelite™.

In all of the silicon doped calcium phosphate materials, Si^{4+} is thought to substitute at P^{5+} sites, requiring an additional nearby charged defect in order to maintain local charge neutrality. The charge compensation mechanisms by which this occurs are difficult to determine due to the small amount of silicon added to these materials. In this paper various possible charge compensation mechanisms are investigated by performing ^{29}Si magic-angle-spinning nuclear magnetic resonance (MAS NMR) spectroscopy on Skelite™, single phase Si-HA and single phase silicon substituted α-tricalcium phosphate, all made using isotopically enriched Si and production techniques similar to those developed for Skelite™. Previous studies have used ab initio calculations to examine possible stable structures for silicon complexes in both Si-HA [14] and Si-TCP [15]. The structures predicted by these investigations form the basis for interpreting the NMR results.

For Si-HA, the ab initio studies [14] examined three possible charge compensation mechanisms: a OH vacancy, an excess hydrogen forming either an $HSiO_4^{3-}$ or HPO_4^{2-} structure and an oxygen vacancy for every two silicon substitutions leading to a $Si_2O_7^{6-}$ complex. Since the different systems contain different numbers and types of atoms, the formation energies could not be compared directly. However, it was noted that the different mechanisms were a hydration sequence in which the addition of a water molecule produced the next structure. This allowed the energies to be compared as a function of water chemical potential, and it was found that for large values of the water chemical potential, i.e. hydrating conditions, the formation of an $HSiO_4$ complex is most stable while for smaller values of the chemical potential, charge compensation by a OH vacancy is most stable. The oxygen vacancy mechanism was found always to have an additional energy cost, but if the energy of formation were slightly lower than calculated this structure would be most stable for an intermediate range of the water chemical potential.

Similar calculations on silicon stabilized α-TCP [15] studied charge compensation for a Si for P substitution by an oxygen vacancy leading to the formation of a Si_2O_7 complex, and one in which an excess calcium compensated for two silicons. For the oxygen vacancy case, structures were found to be much more stable when the two silicate groups joined to form Si_2O_7 compared to situations in which they remained isolated. It was also noted that if every pair of phosphates were replaced by Si_2O_7 the resulting composition, $Ca_3Si_2O_7$, would be that of the mineral rankinite, which has a monoclinic structure with the same space group as α-TCP($P2_1/a$) [16, 17], suggesting that the Si_2O_7 complex obtained in Si-TCP might be similar to that found in rankinite.

For charge compensation with an excess calcium, the investigation focused on a region of the α-TCP structure where a vacant cation site existed between two phosphates. If these two phosphates are replaced by silicates the vacancy provides a natural site for a charge compensating excess Ca. Replacing all pairs of phosphates with this complex yields dicalcium silicate, Ca_2SiO_4, the β phase of which, the mineral larnite, has the same monoclinic structure as α-TCP [18, 19]. This again suggests that the larnite structure should be a good model for this charge compensation mechanism. The energies of the most stable structures for the oxygen vacancy and excess Ca charge compensation mechanisms were compared and it was found that the latter was more stable.

The next section describes the methods developed to produce materials suitable for examination using NMR spectroscopy as well as the characterization of these materials using other analytical methods. This is followed by presentations of the NMR results and a discussion of their interpretation. Conclusions and some recommendations for further investigations complete the paper.

2 Materials preparation and characterization

Due to the low levels of Si doping of the materials of interest and the low natural abundance of the NMR active ^{29}Si, methods were devised to prepare and characterize materials made using a source of enriched ^{29}Si. The materials were produced following the general procedures described by Langstaff et al. [11], Sayer et al. [20], Reid et al. [21] and McLean [22]. A fine colloidal CaP precipitate was prepared by adding an ammoniated solution of ammonium phosphate drop-wise to an ammoniated solution of calcium nitrate with constant mixing and a pH greater than 10 using the reaction:

$$5Ca(NO_3)_2 + 3NH_4H_2PO_4 + 7NH_4OH \rightleftharpoons Ca_5(PO_4)_3OH + 10NH_4NO_3 + 6H_2O$$

Isotopically enriched silicon in the form of a finely dispersed fumed silica colloid (Cab-o-Sperse™ A105 [23]) used in the previous work [11, 20–22] was not available.

The best alternative was found to be silica powder enriched to >96% ^{29}Si (Cambridge Isotope Laboratories product SILM-1076 [24]). In order to ensure that the production was reproducible with this change in silicon source, testing was performed with non-enriched silica powder. The silica powder was added while rapidly mixing the precipitate in order to ensure an even dispersion of silicon. The resulting sol was then aged for 22 h after which the doped precipitates were centrifuged and decanted twice and then dried. The resulting powders were sintered in open alumina crucibles. The heating profile was as follows: the powders were first calcined at 200°C for 3 h, then held at 550°C for 1 h to remove water and NO_2 associated with the initial ingredients and finally sintered for 2 h at 1050°C for the Skelite™ and Si-HA samples and at 1250°C for the Si-α-TCP samples. The ramp rate used throughout the sintering profile was 5°C/min. The final composition of the material was controlled by altering the sintering temperature as well as the relative quantities of the initial constituents—ammonium phosphate, calcium nitrate, and silica—in order to obtain varying molar ratios of Ca/(P + Si) and doping levels. These values for the three materials studied in this work are summarized in Table 1.

The established production methods spray dry the CaP precipitate to give a consistent powder particle size and morphology for further ceramic processing. However, in this study the powders were examined as is. Since some material is lost by spray drying, alternatives to spray drying were investigated in order to preserve as much material as possible. These included drying in air in a furnace at approximately 130°C. After drying, the powder was ground using an alumina mortar and pestle and then sintered.

Skelite™ was produced using non-enriched silica powder with the expected composition: approximately 80 wt% α-TCP with the remainder HA and little to no β-TCP. The preparation of single phase Si-α-TCP with the silica powder was more troublesome. Early attempts using air drying yielded much smaller proportions of the Si-α-TCP phase than the single phase material reported by Reid et al. [21]. A return to spray drying gave better results yielding 93 wt% Si-α-TCP but the cost was roughly half the powder lost.

The production of single phase Si-HA using the precipitation reaction required a Ca/(P + Si) ratio of 1.90 rather the stoichiometric ratio of 1.67 [22]. When the stoichiometric ratio is adopted, a significant quantity of Si-α-TCP is also produced. Trials using silica powder as the silicon source along with spray drying gave Si-HA yields consistently in excess of 95 wt%.

Based on the trials using non-enriched silica, the three materials were produced using enriched silica powder with proportions of calcium, phosphorus and silicon as given in Table 1 with one exception. For the Skelite™ material the Ca/P ratio was increased from 1.67 to 1.70. This was done because Reid et al. [25] has shown that this increase greatly enhances the stability of the phase composition of Skelite™ in the presence of trace amounts of magnesium which is known to nucleate the β-TCP phase. Also, due to the large amount of silicon added to Skelite™ and the high cost of the enriched silica, only one quarter of the silica was enriched while the rest was the un-enriched silica powder used for testing. This still resulted in about 1.3 wt% ^{29}Si in this material, slightly more than in the Si-α-TCP and Si-HA samples.

The three materials produced with the isotopically enriched silica source were analyzed using Rietveld refinement of X-ray powder diffraction data to determine the phase composition and lattice parameters [26], and X-ray fluorescence spectroscopy to determine their elemental composition. All spectra were consistent with data presented earlier [20, 21, 26]. The results for the phase compositions are listed in Table 2.

The lattice parameters were refined for the major constituent phases of the three materials with the results listed in Tables 3 and 4 for the TCP phase and Si-HA, respectively. Also shown in Table 3 are the expected values for α-TCP [27], Si-α-TCP [21] and the Si-TCP$_{sat}$ phase in Skelite™ [20], as measured in the previous studies. Si-α-TCP shows similar trends in lattice parameters compared with pure α-TCP as observed previously by Reid et al. [21] although the *a*-axis lattice parameter has decreased more than was found by Reid et al. and the increases in *b* and β are slightly smaller. The results for the Si-TCP phase in Skelite™ are also close to what was expected. The *a*-axis lattice parameter has decreased but not as much as expected while the *b*-axis and β parameters have increased less than previously observed and *c* is very close to the expected value. Table 4 shows the reported values for HA for both

Table 1 Relevant values for producing Si-α-TCP, Skelite™ and Si-HA

Material	Ca/(P + Si)	Si (wt%)	Ca/P	Sintering Temp. (°C)
Si-α-TCP	1.50	0.87	1.58	1250
Skelite™	1.25	4.90	1.67	1050
Si-HA	1.90	0.87	2.01	1050

Table 2 Phase compositions, in wt%, as determined by Rietveld refinement of X-ray powder diffraction data for Si-α-TCP, Si-HA and Skelite™ made with isotopically enriched silica powder

Material	α-TCP	HA	β-TCP
Si-α-TCP	90	10	0
Si-HA	5	94	1
Skelite™	78	21	1

The uncertainties are estimated to be ±3 wt% [26]

Table 3 Expected lattice parameters for α-TCP [27], Si-α-TCP [21] and Si-TCP_{sat} [20] as well as the values determined from Rietveld analysis of X-ray powder diffraction data for the α-TCP phase in the Si-α-TCP and Skelite™ materials made with enriched silica powder

Material	*a* (Å)	*b* (Å)	*c* (Å)	*β* (°)	Volume (Å^3)
Expected					
α-TCP	12.887	27.280	15.219	126.20	4317.52
Si-α-TCP	12.875	27.370	15.225	126.38	4319.46
Si-TCP_{sat}	12.863	27.357	15.232	126.30	4319.80
Measured					
Si-α-TCP	12.8688 (3)	27.3585 (5)	15.2264 (3)	126.37 (1)	4316.5 (4)
Skelite™	12.8682 (8)	27.335 (1)	15.2329 (8)	126.34 (2)	4316.2 (9)

Table 4 Expected lattice parameters for HA (Holly Springs and NIST) [28, 29] and Si-HA in Skelite™ [20] as well as the values determined from Rietveld analysis of X-ray powder diffraction data for the HA phases in the Si-HA and Skelite™ materials made with enriched silica powder

Material	*a* (Å)	*c* (Å)	Volume (Å^3)
Expected			
Holly Springs HA	9.424	6.879	529.08
NIST HA	9.4225	6.885	529.39
Si-HA (Skelite™)	9.435	6.94	535.02
Measured			
Si-HA	9.4198 (1)	6.8875 (1)	529.26 (1)
Skelite™	9.4289 (5)	6.9345 (6)	533.9 (1)

the Holly Springs material examined by Sudarsanan and Young [28], NIST standard reference material [29] and the HA phase in Skelite™ [20], along with the values found in the present study for single phase Si-HA and the HA phase in Skelite™. For single phase Si-HA, no significant changes in the lattice parameters were observed in comparison to pure HA. For the HA phase within Skelite™ the *a*-axis lattice parameter was slightly larger than for the NIST HA and the single phase Si-HA and there is a significant increase in the *c*-axis parameter giving an overall increase in the unit cell volume. These trends are consistent with what was previously observed in this material by Sayer et al. [20] but the change in *a* is not as large (an increase of 0.0064 Å with respect to NIST HA compared to 0.0125 Å previously observed).

The elemental compositions of the three materials were determined using X-ray fluorescence spectroscopy, carried out by SGS Minerals Services [30]. The results are summarized in Table 5 along with the expected, as-prepared values. All samples were measured in duplicate with the average values for the two measurements reported. The largest disagreement for the two measurements was around 5% with the difference typically being much less than 1%. An uncertainty of 5% was used for the initially measured elemental contents and used to calculate the overall uncertainty in the values presented.

For Si-α-TCP, the molar ratios for both Ca/P and Ca/(P + Si) agree, within error, with the expected values but there was significantly less Si in the material than expected. This could be related to the large amount of HA phase found in this material (10 wt%). The Si-HA material also showed discrepancies between the as-prepared and measured values. The silicon content is significantly higher than expected while both the Ca/P and Ca/(P + Si) ratios are smaller. Interestingly, the Ca/(P + Si) molar ratio is very close to 1.67, which is the expected value for Si-HA. This is similar to the result reported by McLean [22]. For Skelite™, the molar ratios are similar to the expected values with a slightly lower Ca/P ratio compared to the as-prepared value. In the Si-α-TCP material, the silicon content is also significantly lower than expected.

Although there are some differences, the Si-α-TCP, Si-HA and Skelite™ materials manufactured using silica powder enriched with ^{29}Si rather than using Cab-o-Skelite™ are structurally similar to previously studied materials [20, 21, 26]. The only shortcomings being that the Si-α-TCP material was not single phase, instead containing 10 wt% HA, and the Si-HA contained about 5 wt% α-TCP-like phase. These unwanted phases were deemed insignificant for the NMR study as the vast majority of the material was of the desired phase. Furthermore, the Rietveld refinements of the powder XRD spectra which were used to determine the lattice parameters of the various phases

Table 5 As-prepared and XRF measured elemental compositions

Material	Si (wt%)		Ca/(P + Si)		Ca/P	
	As-prepared	Measured	As-prepared	Measured	As-prepared	Measured
Si-α-TCP	0.87	0.70 (5)	1.50	1.53 (4)	1.58	1.59 (4)
Si-HA	0.87	0.99 (5)	1.90	1.65 (4)	2.01	1.75 (4)
Skelite™	4.90	4.58 (5)	1.27	1.27 (4)	1.70	1.65 (4)

showed the anticipated changes in these values, and it is expected that the Si complexes in the materials will be representative of the complexes in the previously studied materials [20, 21, 26].

3 ^{29}Si NMR study

Solid-state ^{29}Si NMR spectra were recorded on a Bruker Avance-500 NMR spectrometer operating at 99.297 MHz for ^{29}Si nuclei ($B_0 = 11.75$ T) under the magic angle spinning condition. A 4 mm Bruker MAS probe was used. A single-pulse excitation was used with a 90° pulse of 4.0 μs and a recycle delay of 30 s. Typically, a sample spinning frequency of 10 kHz was used and 7000–8000 transients were acquired. The free induction decay signal was Fourier transformed to give the spectrum. All ^{29}Si chemical shifts are referenced to tetramethyl silane (TMS) at $\delta = 0$ ppm.

The ^{29}Si MAS NMR spectrum for enriched Si-α-TCP sample is shown in Fig. 1. Two close but distinct peaks are seen: one sharp peak at a chemical shift of approximately −75 ppm with respect to TMS and a second much broader peak around −78 ppm that slightly overlapped the first. Figure 1 also shows Gaussian line profiles fitted to the spectrum using the NUTS NMR data processing software from Acorn NMR Inc. [31]. The resulting peak centroids, breadths, normalized intensities and relative integrated intensities are summarized in Table 6, along with values for the Si-HA and Skelite™ spectra.

The ^{29}Si MAS NMR spectrum for Si-HA is shown in Fig. 2. A single peak is seen centered at −78.2 ppm with a full-width at half-maximum of 2.3 ppm. The corresponding spectrum for Skelite™ shown in Fig. 3 is more complicated. There are two distinct single peaks at approximately −80 and −90 ppm as well as a large signal between −100 and −130 ppm consisting of multiple broad peaks. In all, a total of five Gaussian peaks were fit to this spectrum as shown with the peak properties summarized in Table 6.

With Si substituting for P in these CP materials the chemical shifts are largely determined by the number of coordinating oxygens. For silicon oxides, shifts on the order of 50 ppm are found as the oxygen coordination increases from 4 to 5 and then 6 with values around −100 ppm for SiO_4, the species of interest in this work. Following the approach of Mägi et al. [32] in the assessment of ranges of ^{29}Si chemical shifts for silicates of different Q^n, the corresponding ranges have been estimated for silicates in which the surrounding cations are Ca^{++} with values taken from a number of sources [32–35]. These results for calcium silicates which are illustrated in Fig. 4, give ranges of chemical shift: for a Q^0 of −70 to −75 ppm, for a Q^1 structure −75 to −83 ppm, for a Q^2 structure −84 to −92 ppm, for a Q^3 structure about −100 ppm, and for a Q^4 or silica structure approximately −105 to −120 ppm. This information allows differentiation between the signals of some of the possible charge compensation mechanisms. The mechanism in which two SiO_4 groups are compensated by an oxygen vacancy forms a Si_2O_7 Q^1 complex while

Table 6 Properties of the Gaussian peaks fit to the NMR spectra for Si-α-TCP, Si-HA and Skelite™

Centroid (ppm)	Breadth (ppm)	Normalized amplitude	Relative integrated intensity
Si-α-TCP			
−75.2	1.5	100	28.5
−78.0	5.2	74.7	71.5
Si-HA			
−78.2	2.3	100	100
Skelite™			
−78.9	2.1	45.4	6.7
−90.9	1.6	36.7	4.1
−106.7	5.0	21.3	7.2
−112.8	1.7	32.7	3.8
−118.4	11.4	100	78.2

The peak centroids, breadths, normalized amplitudes and relative integrated intensities are given for each spectrum

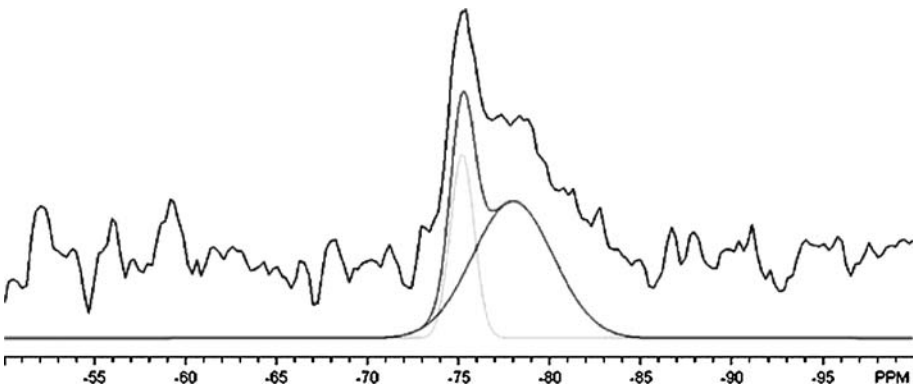

Fig. 1 The ^{29}Si MAS NMR spectrum for Si-α-TCP with fitted peaks

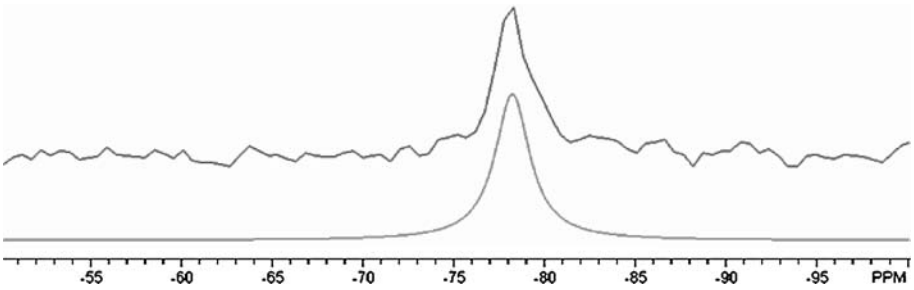

Fig. 2 The ^{29}Si MAS NMR spectrum for Si-HA with fitted peak

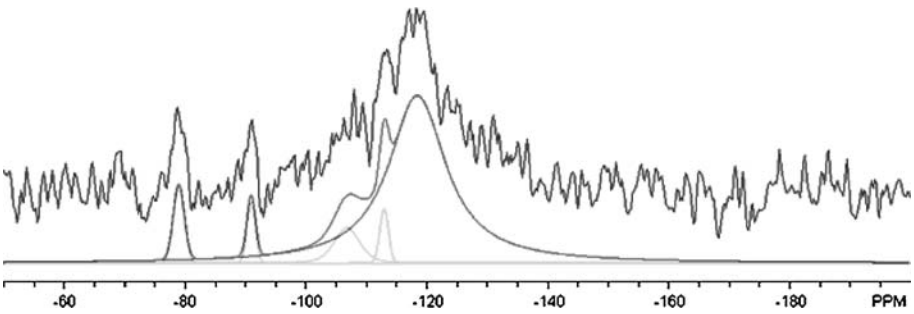

Fig. 3 The ^{29}Si MAS NMR spectrum for Skelite^{TM} with fitted peaks

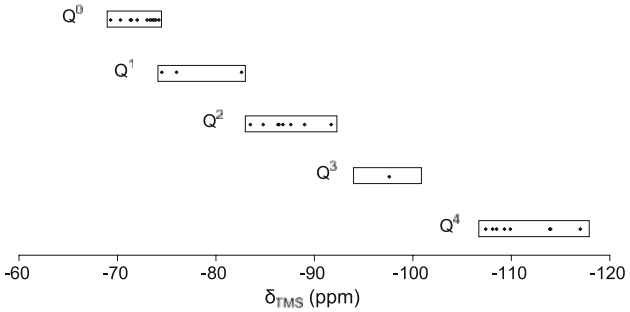

Fig. 4 Ranges of chemical shifts in calcium silicates with varying degrees of condensation of tetrahedra. Chemical shift values obtained from [32–35]

compensation by either excess calcium, excess hydrogen or a OH vacancy all result in a Q^0 type complex.

The smaller changes observed within silicate groups with the same Q^n value are due to distortions in the local structure. For instance, Si–O bond lengths, O–Si–O bond angle distortions from the ideal tetrahedral value, the length and number of bonds between the oxygens of the tetrahedra and the calcium cations and the Si–O–Si bond angle in condensed structures all have a small effect on the chemical shift in the order of a few ppm. For example, in the dicalcium silicate minerals (Ca_2SiO_4) the chemical shift for the Q^0 silicon site is −70.3, −71.4 and −73.5 ppm for the α, β and γ phases respectively, and for the mineral rankinite ($Ca_3Si_2O_7$) chemical shifts of −74.5 and −76.0 ppm are found for the Q^1 Si_2O_7 structure in which the two silicon sites are not geometrically equivalent.

A detailed empirical relationship relating silicate structural parameters to the chemical shift has been developed by Sherriff et al. [36, 37]. It involves five structural parameters and takes into account the second nearest neighbour cations to the silicon atom. The final relationship for the chemical shift was obtained from a least-squares refinement on 72 silicate structures containing 124 unique silicon sites in which the NMR chemical shift and accurate structural models based on X-ray and Neutron diffraction were known. For the 124 silicon sites a root mean square deviation of 0.66 ppm was obtained between the predicted and measured chemical shift values with a maximum disagreement of less than 4 ppm for Q^0 and Q^1 structures.

The empirical relationship developed by Sherriff et al. [37] was used to calculate expected chemical shifts for the various possible silicon structures obtained from the fully relaxed ab initio calculations of Astala et al. [14] for silicon doped hydroxyapatite, and of Yin and Stott [15] for silicon stabilized α-tricalcium phosphate. Table 7 shows these results for three candidate structures in Si-HA: charge compensation of silicon replacing phosphorus via an excess hydrogen, a OH vacancy or an oxygen vacancy for every two silicons, and two such structures in silicon stabilized α-tricalcium phosphate: charge compensation by an excess calcium and by an oxygen vacancy. Also listed in Table 7 are experimentally determined values and values calculated using the relationship of Sherriff et al. [37] for the calcium silicate minerals larnite and rankinite which should have similar silicon structures to those in silicon doped α-TCP for the excess calcium and oxygen vacancy charge compensation mechanisms respectively. The difference between the predicted chemical shifts and observed values for these two materials ranges between 1 and 3 ppm which provides a measure of confidence in the approach.

Table 7 ^{29}Si NMR chemical shifts predicted by the empirical model of Sherriff et al. [37] for the possible silicon structures in Si-HA found by Astala et al. [14], for the most energetically favourable silicon structures in Si-α-TCP found by Yin and Stott [15], and for the minerals larnite and rankinite for which measured values are also given [32]

Material	Charge compensation mechanism	Q^n structure type	Predicted chemical shift (ppm)	Measured chemical shift (ppm)
Si-HA	Excess H	Q^0	−65.9	
	OH Vacancy	Q^0	−69.6, −66.2	
	O Vacancy	Q^1	−74.9, −68.3	
Si-α-TCP	Excess Ca	Q^0	−69.9, −73.3	
	O Vacancy	Q^1	−81.1, −71.1	
Larnite		Q^0	−70.4	−71.4
Rankinite		Q^1	−76.3, −78.4	−74.5, −76.0

In the case of the Si-HA system both the excess hydrogen and OH vacancy mechanisms result in a Q^0 type silicate structure while the oxygen vacancy mechanism gives a Q^1 structure. The first of the two values (−69.6 ppm) reported for the OH vacancy is for the more stable structure in which the OH vacancy is in the same plane as the Si. The two values listed for the oxygen vacancy mechanism correspond to the two different silicon sites in the Si_2O_7 structure. The three Q^0 structures that were calculated (one for an excess hydrogen and two different OH vacancy structures) all fall slightly below but close to the range expected for this type of structure in calcium silicates (see Fig. 4). For the Q^1 Si_2O_7 structure, one silicon site is predicted to have a chemical shift at the lower end of the expected range whereas the second silicon site is significantly less shielded than expected for this type of structure. One unusual feature of this second site was that one of the oxygen atoms of the silicate group had only two nearest neighbour calcium cations, while in almost all of the other structures examined there were at least three oxygen-cation bonds. Each of these bonds increased the predicted chemical shielding of the silicon nucleus so having one less bond helps to explain the predicted value falling outside of the expected range for a Q^1 structure.

In the case of silicon stabilized α-TCP, calculated chemical shift values are shown in Table 7 for two distinct silicon structures for each of the two charge compensation mechanisms. Both values for the Q^0 type structure of the excess calcium mechanism fall within the expected Q^0 range while one of the values for the Q^1 oxygen vacancy structure is within the expected range but the other is at a less shielded value. Due to the complexity of the α-TCP structure there were many ways to create both of the possible structures by substituting silicon at different phosphorus sites. The three most energetically favourable locations for each of the complexes were examined. For the excess calcium complex, these six silicon sites had a predicted chemical shift range of −69.3 to −75.0 ppm and an average value of −72.1 ppm. For the Si_2O_7 complexes, the six silicon sites had a range of predicted chemical shifts between −70.4 and −81.1 ppm and an average value of −75.7 ppm.

4 Discussion

The survey of silicon chemical shifts in calcium silicate structures, summarized in Fig. 4, and the calculations performed using the empirical model of Sherriff et al. [37] allows some conclusions to be drawn as to the likely origins of the measured ^{29}Si NMR spectra.

4.1 Si-HA

Based on the chemical shifts of other calcium silicate structures the single peak in the Si-HA NMR spectrum at −78.2 ppm suggests a Q_1 structure. Of the three possible charge compensation mechanisms treated by Astala et al. [14] for this material, namely an excess hydrogen, OH vacancy and O vacancy, only the latter gives a Q^1 structure. The OH vacancy and the excess hydrogen complexes give Q^0 structures, although in the latter case one of the oxygens is replaced by a hydroxyl. A similar structure in which an oxygen is replaced by a hydroxyl in a Q^0 type silicate is found in the mineral afwillite ($Ca_3(HSiO_4) \cdot 2H_2O$) [38] for which the two different silicon sites in this material have measured chemical shifts of −71.3 and −73.3 ppm [33], within the range expected for Q^0 calcium silicates without hydroxyl groups. The results in Table 7 using the model of Sherriff et al. [37] for the three structures did not give any chemical shifts that agreed closely with the observed value of −78.2 ppm. The closest value was for the oxygen vacancy, with predicted chemical shifts of −68.3 and −74.9 ppm for the two different silicon sites. None of the other possible structures had predictions within 8 ppm of the observed value. Based on these observations of chemical shifts in other calcium silicates and the values predicted by the model of Sherriff et al. [37] it seems that the silicon structure in the Si-HA material is most likely a Q^1 structure in which the substitution of two adjacent phosphate groups by silicates is charge compensated by an oxygen vacancy resulting in a Si_2O_7 structure.

This is the only direct experimental evidence for this type of structure in silicon doped hydroxyapatite. Previous studies of Si-HA produced using a variety of methods

suggested both a OH vacancy [39–41] and excess hydrogen [42] as the charge compensating mechanism. The theoretical study of Astala et al. [14], which examined all three of these possible mechanisms, found the oxygen vacancy structure to be less energetically favourable than the other two. But, the most stable structure was dependent on the water chemical potential and there was a small intermediate range of chemical potential over which this structure would be stable if the calculated formation energy had been slightly lower. This dependence on the water chemical potential could possibly explain the different structures reported in the various studies that have been performed due to differences in the production method.

4.2 Si-α-TCP

There are two peaks in the ^{29}Si NMR results for the Si-α-TCP material. The broad peak at −78.0 ppm is very close to the peak in Si-HA which may correspond to the small amount (10 wt%) of the HA phase in the sample. However, the breadth of this peak at −78.0 ppm results in a much larger integrated intensity for it than for the sharper peak at 75.2 ppm. If the peak at −78.0 ppm were due to such a small amount of the HA phase, this phase would have to contain 7 wt% silicon while the Si-α-TCP phase would contain less than 0.5 wt% silicon. This is not likely as most studies estimate that Si-HA reaches saturation at around 1 wt% silicon. Also, the much larger breadth compared to the peak in Si-HA suggests different origins.

Reference to Fig. 4 indicates that the peak centred at −78.0 ppm is due to a Q^1 silicate structure. The sharper peak at −75.2 ppm is more difficult to interpret and could be associated with either Q^0 or Q^1 structures. The two charge compensation mechanisms considered by Yin and Stott [15] for silicon doped tricalcium phosphate were compensation for every two silicon impurities by either an excess calcium, forming Q^0 structures, or an oxygen vacancy, giving a Q^1 structure. The position of the second peak at −75.2 ppm is in better agreement with the calculated value in Table 7 for the oxygen vacancy mechanism. When the three most stable structures for each complex are considered, the average calculated chemical shift for the six silicon sites are −72.1 and −75.7 ppm for the excess calcium and oxygen vacancy mechanisms respectively also suggesting the oxygen vacancy mechanism for the peak at −75.2 ppm. Finally, the chemical shifts of the two calcium silicate minerals with similar structures to these two mechanisms are −71.4 ppm for larnite (indicative of the excess calcium complex) and −74.5 and −76.0 ppm for rankinite (oxygen vacancy complex). Overall, it is very likely that both peaks in the Si-α-TCP spectrum are due to Q^1 complexes with charge compensation provided by the creation of oxygen vacancies and the formation of Si_2O_7. That there are multiple peaks in the Si-α-TCP spectrum, one being very broad, means there are several structurally different Si_2O_7 sites. The site responsible for the sharp peak at −75.2 ppm must be a preferred site while the broad peak centred at −78.0 ppm is likely due to a group of sites with slight variations in structure. In contrast, only a single sharp peak was observed for Si-HA. Whereas in HA there is only a single distinct phosphorus site as the six phosphorus atoms in the unit cell are related through symmetry, in α-TCP there are twelve distinct phosphorus sites giving many possibilities for the substitution of silicon and the formation of different Si_2O_7 complexes.

The presence of multiple peaks for the Si-α-TCP sample may also explain the behaviour of the *a* lattice parameter in this material observed by Reid et al. [21]. This was found to decrease significantly from the value in pure α-TCP upon first addition of silicon, followed by a partial recovery and then a plateau at a doping level of around 1 wt%. In contrast, both the *b* and *β* lattice parameters changed linearly with additional silicon until approximately 1 wt% silicon doping at which point they also plateaued. This indicates that there may be different silicon structures forming at different doping levels which have different effects on the *a* lattice parameter.

4.3 Skelite™

The ^{29}Si NMR spectrum for Skelite™, shown in Fig. 3, is more complicated with five distinct peaks fit to the data. The three peaks fit between −105 and −120 ppm are barely distinguishable and were only fit separately to facilitate an accurate integrated intensity. These peaks are characteristic of a Q^4 or SiO_2 structure, but as no such crystalline phases were seen in the X-ray powder diffraction results these are likely due to an amorphous phase observed previously in this material [20, 43]. A second X-ray powder diffraction scan with 12 wt% silicon standard [29] added was performed and the phase composition was determined to be 14 wt% HA, 66 wt% α-TCP, 4 wt% *β*-TCP and 16 wt% amorphous phase which is similar to the compositions found by Sayer et al. [20] for the same material made using a fumed silica colloid. The width of these peaks, especially that at −118 ppm are also indicative of small variations in the environment of the silicon atoms that is to be expected in an amorphous material.

The combined integrated intensities of the Q^4 type structure peaks suggests that almost 90% of the added silicon does not diffuse into the crystalline phases but forms an amorphous phase. However, this may be an overestimate since two different silicon sources were used for this material as discussed earlier, and it is possible that the non-enriched silica diffused preferentially into the crystalline

phases excluding the enriched silica, which is predominantly what is measured in the NMR experiment.

The large proportion of silicon not incorporated into the crystalline phases makes the interpretation of the other peaks difficult. The amount of silicon in these phases is slightly more than in the single phase materials based on the observed lattice parameter changes, but only one quarter of the silicon in this material was isotopically enriched. This resulted in a fairly small signal to noise ratio for the peaks at −78.9 and −90.9 ppm, making the determination of the centres and widths of these peaks less precise. This is unfortunate as the former peak coincides in position with one observed in both the single phase Si-HA and Si-α-TCP samples. The peak at −90.9 ppm is characteristic of a Q^2 structure from either a chain or ring silicate but neither of these structures are likely to be present in Si-HA or Si-TCP because the severe distortion of the crystal structure they would cause was not detected in the X-ray diffraction spectrum. Changes in the lattice parameters for both of these phases indicate both contain silicon, which means that the entire signal from silicon that has diffused into the HA and TCP phases is contained in the peak at −78.9 ppm or possibly another small, broad peak indistinguishable from the background. This is once again indicative of a Q^1 structure suggesting that oxygen vacancies are compensating for the replacement of phosphorus by silicon.

The origin of the peak at −90.9 ppm is uncertain. Two possibilities are silicon in an amorphous phase, or more likely because of the narrowness of the peak (1.6 ppm FWHM), the presence of a crystalline calcium silicate. However, there are no reports of ^{29}Si MAS NMR peaks for calcium silicate structures matching this position. The closest match was for the mineral wollastonite ($Ca_3Si_3O_9$) which contains chains made up of three connected SiO_4 tetrahedra [44] and gives two separate peaks in the NMR spectrum: a peak at −91.7 ppm and a peak of half the intensity at −87.6 ppm. But, no such crystalline phase was detected in the X-ray powder diffraction spectrum although this may simply be due to the small quantity of this phase present.

5 Conclusions

Three silicon-doped calcium phosphate biomaterials have been investigated using ^{29}Si MAS NMR in order to determine the nature of the silicon complexes and the mechanisms of charge compensation for Si in these systems. Si-HA, Si-α-TCP and Skelite™ were prepared using isotopically enriched Si as the dopant. The methods for preparing the samples differed slightly from previous methods because the enriched Si was only available in the form of silica powder rather than the dispersed fumed silica colloid (Cab-o-Sperse™) of the earlier methods, but characterisation of the samples showed that satisfactory materials were obtained. The ^{29}Si NMR spectra showed a single narrow peak for Si-HA, a narrow and a broad peak for Si-α-TCP and many peaks for the Skelite™ sample. A survey of the ranges of chemical shifts exhibited by calcium silicate materials, and shifts calculated using the empirical formula of Sherriff et al. [36, 37] with atomic structures of Si complexes obtained from ab initio simulations of these systems [14, 15] were used to interpret the NMR spectra. A signal of the Q^1 type was found in each of the materials which corresponds to two silicate units sharing an oxygen. The only charge compensation mechanism of those considered previously which gives a Q^1 structure is compensation by an oxygen vacancy with the resulting formation of a Si_2O_7.

An oxygen vacancy charge compensation mechanism in Si-HA raises the possibility that it could be responsible for the conversion of HA to TCP as this is also a charge compensation mechanism observed in the Si-TCP phase. The dehydration of the apatite phase, which is a necessary step for the conversion to occur, may simply be a result of the sintering at high temperature, or could possibly be a secondary effect of the oxygen vacancy charge compensating defect. Previous experimental studies of single phase Si-HA [39–42] have found evidence of various charge compensation mechanisms but not the oxygen vacancy mechanism found here. The material production methods used in these other studies also did not yield a Si-TCP phase. It seems likely that the charge compensation mechanisms, phase composition and other aspects of the Si-HA and the other materials is affected by the details of their preparation, for example the humidity and sintering temperature. This view is supported by Astala and coworkers [14, 15] who concluded that the energetically favourable charge compensation mechanism in Si-HA depends on the water chemical potential which is determined by the temperature and water partial pressure.

Acknowledgements Work supported by the NSERC of Canada and Millenium Biologix Inc. Many discussions with Joel Reid are gratefully acknowledged.

References

1. Bohner M. Calcium orthophosphates in medicine: from ceramics to calcium phosphate cements. Injury. 2000;31:D37–47.
2. Vallet-Regí M, González-Calbet JM. Calcium phosphates as substitution of bone tissues. Prog Solid State Chem. 2004; 32:1–31.
3. Hench L. Bioceramics: from concept to clinic. J Am Ceram Soc. 1991;74:1487–510.
4. Ducheyne P, Radin S, King L. The effect of calcium-phosphate ceramic composition and structure on in vitro behaviour. J Biomed Mater Res. 1993;27:25–34.

5. Porter AE, Patel N, Skepper JN, Best SM, Bonfield W. Comparison of in vivo dissolution processes in hydroxyapatite and Si-substituted hydroxyapatite bioceramics. Biomaterials. 2003; 24:4609–20.
6. Patel N, Gibson IR, Hing KA, Best SM, Revell PA, Bonfield W. A comparative study on the in vivo behaviour of hydroxyapatite and Si-substituted hydroxyapatite granules. J Mater Sci: Mater Med. 2002;13:1199–206.
7. Carlisle EM. Silicon: an essential element for the chick. Science. 1972;178:619–21.
8. Carlisle EM. Silicon: a possible factor in bone calcification. Science. 1970;167:279–80.
9. Qiu Q, Vincent P, Lowenberg B, Sayer M, Davies JE. Bone growth on sol–gel calcium phosphate thin films in vitro. Cells Mater. 1993;3:351–60.
10. Davies JE, Shapiro G, Lowenberg B. Osteoclastic resorption of calcium phosphate ceramic thin films. Cells Mater. 1993;3: 245–56.
11. Langstaff S, Sayer M, Smith TJN, Pugh SM, Hesp SAM, Thompson WT. Resorbable bioceramics based on stabilized calcium phosphates. Part I. Rational design, sample preparation and material characterization. Biomaterials. 1999;20:1727–41.
12. Langstaff S, Sayer M, Smith TJN, Pugh SM. Resorbable bioceramics based on stabilized calcium phosphates. Part II. Evaluation of biological response. Biomaterials. 2001;22:135–50.
13. Pietak AM. The role of silicon in the bioactivity of Skelite™ bioceramic. A material and biological characterization of silicon α-tricalcium phosphate based ceramics. Master's thesis, Queen's University; 2007.
14. Astala R, Calderin L, Yin X, Stott MJ. Ab initio simulation of Si-doped hydroxyapatite. Chem Mater. 2006;18:413–22.
15. Yin X, Stott MJ. Theoretical insights into bone grafting silicon-stabilized α-tricalcium phosphate. J Chem Phys. 2005;122 (024709-1).
16. Kusachi I. The structure of rankinite. Mineral J. 1975;8:38–47.
17. Saburi S, Kusachi I, Henmi C, Kawahara A, Henmi K, Kawada I. Refinement of the structure of rankinite. Mineral J. 1976;8:240–6.
18. Midgley CM. The crystal structure of β dicalcium silicate. Acta Crystallogr. 1952;5:307–12.
19. Jost KH, Ziemer B, Seydel R. Redetermination of the structure of β-dicalcium silicate. Acta Crystallogr B 1977;33:1696–700.
20. Sayer M, Stratilatov AD, Reid JW, Calderin L, Stott MJ, Yin X, et al. Structure and composition of silicon-stabilized tricalcium phosphate. Biomaterials. 2003;24:369–82.
21. Reid JW, Tuck L, Sayer M, Fargo K, Hendry JA. Synthesis and characterization of single-phase silicon substituted α-tricalcium phosphate. Biomaterials. 2006;27:2916–25.
22. McLean DA. Osteoblast response on silicon doped calcium phosphate biomaterials. Master's thesis, Queen's University; 2007.
23. Cabot Corporation. 500 Commerce Dr., Aurora, IL. http://www.cabot-corp.com.
24. Cambridge Isotope Laboratories Inc. 50 Frontage Road, Andover, MA. http://www.isotope.com.
25. Reid JW, Fargo K, Hendry JA, Sayer M. The influence of trace magnesium content on the phase composition of silicon-stabilized calcium phosphate powders. Mater Lett. 2007;61:3851–4.
26. Reid JW, Hendry JA. Rapid, accurate phase quantification of multiphase calcium phosphate materials using Rietveld refinement. J Appl Crystallogr. 2006;39:536–43.
27. Mathew M, Schroeder LW, Dickens B, Brown WE. The crystal structure of α-$Ca_3(PO_4)_2$. Acta Crystallogr B. 1977;33:1325–33.
28. Sudarsanan K, Young RA. Significant precision in crystal structural details: holly springs hydroxyapatite. Acta Crystallogr B. 1968;25:1534–43.
29. National Institute of Standards and Technology. Standard reference material 2910. Gaithersburg, MD; 2003.
30. SGS Minerals Service. 185 Concession St. Lakefield, ON. http://www.met.sgs.com.
31. Acorn NMR Inc. 7670 Las Positas Rd., Livermore, CA. http://www.acornnmr.com.
32. Mägi M, Lippmaa E, Samoson A, Engelhardt G, Grimmer AR. Solid-state high-resolution silicon-29 Chemical shifts in silicates. J Phys Chem. 1984;88:1518–22.
33. Engelhardt G, Michel D. High-resolution solid-state NMR of silicates and zeolites. John Wiley & Sons; 1987.
34. Stebbins JF. Mineral physics & crystallography. A handbook of physical constants, vol. 2, chapter 14. American Geophysical Union; 1995.
35. MacKenzie KJD, Smith ME. Multinuclear solid-state NMR of inorganic materials. Oxford: Elsevier Science; 2002.
36. Sherriff BL, Grundy HD. Calculations of ^{29}Si MAS NMR chemical shift from silicate mineral structure. Nature. 1988;332: 819–22.
37. Sherriff BL, Grundy HD, Hartman JS. The relationship between ^{29}Si MAS NMR chemical shift and silicate mineral structure. Eur J Mineral. 1991;3:751–68.
38. Malik KMA, Jeffery JW. A re-investigation of the structure of afwillite. Acta Crystallogr B. 1976;32:475–80.
39. Gibson IR, Best SM, Bonfield W. Chemical characterization of silicon-substituted hydroxyapatite. J Biomed Mater Res. 1999; 44:422–8.
40. Leventouri Th, Bunaciu CE, Perdikatsis V. Neutron powder diffraction studies of silicon-substituted hydroxyapatite. Biomaterials. 2003;24:4205–11.
41. Tang XL, Xiao XF, Liu RF. Structural characterization of silicon-substituted hydroxyapatite synthesized by a hydrothermal method. Mater Lett. 2005;59:3841–6.
42. Arcos D, Carvajal JR, Vallet-Regí M. The effect of the silicon incorporation on the hydroxylapatite structure. A neutron diffraction study. Solid State Sci. 2004;6:987–94.
43. Tuck LE. The phase evolution and microstructure of silicon doped tricalcium phosphate. Master's thesis, Queen's University; 2005.
44. Hesse KF. Refinement of the crystal structure of wollastonite-2m (parawollastonite). Zeitschrift für Kristallographie. 1984;168: 93–8.